Research Square

Preprints are preliminary reports that have not undergone peer review.
They should not be considered conclusive, used to inform clinical practice,
or referenced by the media as validated information.

Unveiling the miR-26a-5p/MSMO1/7-DHC Axis: A Novel Therapeutic Target in Myocardial Ischemia-Reperfusion Injury

Yonglin Fu
Guangdong Medical University
Bingjie Han
Kashi Medicine University
Jiankai Zhang
Guangdong Medical University
Lu Liu
Guangdong Medical University
Wenjie Chen
Guangdong Medical University
Ciying Kuang
Guangdong Medical University
Mei Jiang
Guangdong Medical University
Xiaojun Cui
cuixiaojun@gdmu.edu.cn
Guangdong Medical University

Research Article

Keywords: engineered exosomes, miR-26a-5p, MSMO1, 7-DHC, ferroptosis, myocardial ischemia-reperfusion injury

Posted Date: May 11th, 2026

DOI: https://doi.org/10.21203/rs.3.rs-9491112/v1

License: This work is licensed under a Creative Commons Attribution 4.0 International License.
Read Full License

Additional Declarations: No competing interests reported.

Version of Record: A version of this preprint was published at Cardiovascular Drugs and Therapy on August 10th, 2026. See the published version at https://doi.org/10.1007/s10557-026-07922-2.

Abstract

Ferroptosis plays a critical role in myocardial ischemia-reperfusion injury (MIRI). Here, we discovered that MSMO1, a key enzyme in the cholesterol biosynthesis pathway, regulates ferroptosis in MIRI, and identified miR-26a-5p as an upstream regulator of MSMO1. During MIRI, downregulation of miR-26a-5p led to suppression of MSMO1, reduction of 7-DHC accumulation, and promotion of lipid peroxidation and ferroptosis. To translate this mechanism, we developed engineered exosomes delivering miR-26a-5p. In cellular and mouse MIRI models, this intervention significantly improved cardiac function, reduced infarct size, and attenuated fibrosis. This work provides a novel therapeutic strategy for MIRI and validates the clinical potential of engineered exosomes as a cell-free therapeutic platform.

1. Introduction

Ischemic cardiac diseases such as acute myocardial infarction (AMI) and coronary artery disease (CAD) are common clinical conditions and represent one of the leading causes of heart failure (HF), with mortality rates continuing to rise annually[1]. In recent years, with the widespread adoption of percutaneous coronary intervention (PCI), revascularization therapy has enabled the salvage of ischemic myocardium in most patients[2]. However, the restoration of coronary blood flow itself can induce myocardial damage-known as MIRI-for which no effective therapeutic strategy currently exists[3]. Consequently, how to effectively prevent and manage MIRI remains a critical and urgent issue in cardiovascular clinical practice.

Ferroptosis is a major form of cardiomyocyte death during myocardial ischemia-reperfusion injury[4]. Ferroptosis is a regulated form of cell death dependent on iron and reactive oxygen species (ROS), characterized by the peroxidative destruction of phospholipids containing polyunsaturated fatty acyl chains on cellular or organellar membranes following the inactivation of intracellular reductive systems, ultimately leading to cell death[5]. Cholesterol, as a core lipid component of cell membranes, is extensively involved in maintaining membrane fluidity, signal transduction, and energy metabolism regulation in myocardial tissue[6]. Due to the abundance and high metabolic activity of mitochondria in cardiomyocytes, cholesterol homeostasis requires precise regulation through dual pathways-endogenous biosynthesis and exogenous uptake-to maintain a dynamic balance[7, 8]. Studies indicate that cholesterol metabolic dysregulation exerts a dual pathological effect in MIRI. On one hand, cholesterol overload promotes oxidative stress and lipid peroxidation; a high-cholesterol diet significantly elevates serum LDL-C levels, facilitating the deposition of oxidized low-density lipoprotein (ox-LDL) in ischemic myocardium[9, 10]. ox-LDL activates NADPH oxidase via the LOX-1 receptor, leading to a burst of ROS production, exacerbating lipid peroxidation and inducing cardiomyocyte ferroptosis. On the other hand, insufficient cholesterol synthesis weakens the endogenous anti-injury response. Cholesterol participates in the assembly of mitochondrial electron transport chain complexes; its deficiency results in reduced ATP production, aggravating myocardial energy depletion during reperfusion[11–13]. Two studies published in Nature in 2024 revealed the critical role of key enzymes in

the distal segment of the cholesterol biosynthesis pathway in regulating ferroptosis. Distinct from classical ferroptosis mechanisms, this regulation directly influences the structure and function of membrane lipid rafts through modulating endogenous cholesterol synthesis, thereby participating in the pathological progression of ferroptosis[14, 15]. Among these enzymes, MSMO1 exhibits the most prominent ferroptosis-suppressive effect. As a key enzyme in the cholesterol biosynthesis pathway, MSMO1 catalyzes the oxidation of sterol intermediates to ensure proper cholesterol synthesis. Consequently, we turned our focus to investigating how MSMO1 regulates ferroptosis via modulating cholesterol and its metabolite levels.

In recent years, advancements in stem cell regenerative medicine have opened new avenues for the treatment of cardiovascular diseases. Numerous studies have demonstrated that stem cells can promote the repair of damaged myocardial tissue through the paracrine release of exosomes (Exo) and cytokines[16]. Exosomes are extracellular vesicles with a diameter of 100–150 nm. They mediate intercellular communication and play a crucial role in the exchange of cellular materials and signals. Compared with the direct administration of stem cells, the use of stem cell-derived exosomes avoids risks such as immune rejection and tumorigenesis[17, 18]. As natural nanoscale delivery vehicles, exosomes exhibit considerable potential in disease therapy due to their low immunogenicity, high biocompatibility, and inherent targeting capabilities[19]. However, native exosomes present limitations including low drug-loading capacity and insufficient targeting specificity. Engineering exosomes through genetic modification to carry specific therapeutic miRNAs represents a cutting-edge strategy to enhance their therapeutic efficacy and safety[20].

Previous studies have identified miR-26a-5p as a protective factor in cardiovascular diseases[21]. Enhancing the expression of miR-26a-5p in H9C2 cells subjected to hypoxia/reoxygenation (H/R) induction can alleviate H9C2 cell apoptosis and oxidative stress[22]. MSMO1 is a key enzyme in the distal cholesterol biosynthesis pathway. Its regulatory mechanism in MIRI has not been clarified. Meanwhile, miR-26a-5p exerts cardiovascular protective effects, but whether it can ameliorate MIRI by targeting MSMO1 to regulate ferroptosis remains unknown[21]. In this study, we demonstrated that during MIRI, downregulation of miR-26a-5p leads to reduced expression of MSMO1/7-DHC, thereby impairing the endogenous anti-ferroptotic capacity of cardiomyocytes. The delivery of miR-26a-5p via engineered stem cell-derived exosomes effectively attenuates cardiomyocyte ferroptosis by targeting and elevating MSMO1/7-DHC levels, consequently improving MIRI outcomes.

2. Materials and methods

2.1 Preparation of exosomes

Cultured mesenchymal stem cells (MSCs) were grown to the logarithmic growth phase and gently washed with PBS buffer to remove residual culture medium. An appropriate volume of serum-free, exosome-free medium was then added, and the cells were cultured for an additional 24–48 h to promote

the release of secreted factors. Subsequently, cells were removed by centrifugation (1,200 rpm, 5 min), and the supernatant was collected and filtered to eliminate any possible cell debris. The collected MSC-conditioned supernatant was centrifuged (300 rpm, 10 min) to pellet cellular debris. The supernatant was transferred to a new centrifuge tube and subjected to higher-speed centrifugation (2,000 rpm, 10 min) to remove larger particles. This was followed by further centrifugation at 10,000 rpm for 30 min to eliminate additional cell fragments and microvesicles. Finally, the supernatant was transferred to a new tube and ultracentrifuged (100,000 rpm, 2 h). The resulting pellet, containing the exosomes, was collected and stored at -80°C[48].

2.2 Characterization of exosomes

Isolated exosomes were fixed with 1% glutaraldehyde and subsequently applied as a droplet onto Formvar/carbon-coated grids. The grids were negatively stained with 3% aqueous phosphotungstic acid for 1 min and then examined under transmission electron microscopy (TEM) to visualize the morphology of MSC-derived exosomes. For nanoparticle tracking analysis (NTA), purified exosomes were accurately diluted 100- to 1000-fold in sterile PBS, and the diluted sample was injected into the NTA sample cell to determine the particle size distribution and concentration. In addition, immunoblotting was performed using antibodies against the canonical exosomal markers CD9, CD81, TSG101, Alix, and Flot1, as well as the endoplasmic reticulum marker Calnexin (serving as a negative control), to confirm the identity and purity of the isolated vesicles[49].

2.3 Engineering of exosomes

miR-26a-5p mimics (Sangon Biotech, Shanghai, China) and Exo-fect™ reagent were separately diluted in TransSolution in sterile microcentrifuge tubes, gently mixed, and incubated at room temperature for 5 min. The diluted miR-26a-5p mimics and Exo-fect™ solutions were then combined, mixed gently, and further incubated at room temperature for 15 min. Purified exosomes were added to the resulting complex, mixed gently by pipetting, and the exosome-loading mixture was incubated on a shaking incubator at 37°C for 2 h, followed by overnight static incubation at 4°C. Finally, the mixture was loaded onto a centrifugal filtration column and centrifuged to remove unincorporated miR-26a-5p mimics[51]. The sequence used in this study was as follows: miR-26a-5p mimics: UUCAAGUAAUCCAGGAUAGGCU.

2.4 Internalization of engineered exosomes in vitro and in vivo

To evaluate the internalization of engineered exosomes by AC16 cells in vitro, exosomes were labeled with DiR according to the manufacturer's protocol. AC16 cells (1×10^5 cells/mL) were cultured in a 5% CO_2 incubator at 37°C. When cells reached 70% confluence, medium containing DiR-labeled engineered exosomes was added. After 12 h, cells were washed three times with PBS, fixed with 4% paraformaldehyde at 4°C, washed again three times with PBS, and stained with DAPI. Cells were then observed under a confocal fluorescence microscope (ZEISS LSM 980, Germany). For in vivo internalization assessment, DiR-labeled exosomes were administered via tail-vein injection.

Epifluorescence signals were detected at 2, 4, and 24 h post-injection using a small-animal in vivo imaging system (MOIS HT, RWD, China).

2.5 Establishment of cardiomyocyte ischemia-reperfusion injury model

AC16 cardiomyocytes at the logarithmic growth phase were seeded into culture dishes and routinely cultured for 24 h in a humidified incubator at 37°C with 5% CO_2. After drug treatment for 12–24 h, the old medium was removed, and cells were rinsed twice with PBS. Glucose-free and serum-free DMEM medium was then added, and the cells were transferred to a tri-gas incubator (1% O_2, 94% N_2, 5% CO_2) for 6–7 h to simulate ischemia. Subsequently, the medium was replaced with complete DMEM/F12 medium, and the cells were returned to the normoxic incubator (37°C, 5% CO_2) for 10–12 h to mimic reperfusion.

2.6 Establishment of the mouse myocardial ischemia-reperfusion injury model

All animal procedures were performed in accordance with relevant ethical guidelines. The experimental protocol was approved by the Laboratory Animal Center of Guangdong Medical University (Dongguan, China). Thirty adult male C57BL/6 mice were randomly assigned to the following groups: sham-operated, model, exosome-treated, and engineered exosome-treated. Mice were anesthetized by intraperitoneal injection of 1-1.5 ml 1.25% tribromoethanol and placed in the supine position. Following tracheal intubation, mechanical ventilation was maintained with a tidal volume of 0.8 ml. A 0.5 cm incision was made along the left fourth intercostal space to expose the heart. An 8-0 non-traumatic suture was placed under the left atrial appendage to ligate the left anterior descending coronary artery, inducing myocardial ischemia. Electrocardiographic monitoring (YuYan, China) was performed throughout the procedure. After 20 min of ischemia, the ligature was released to restore coronary flow, and the incision was sutured. Sham-operated mice underwent identical procedures except for coronary ligation. Upon reperfusion, sham and model groups received 100 μl PBS via tail-vein injection, while the treatment groups received 100 μl of either exosomes or engineered exosomes immediately at the onset of reperfusion (within 5 min after release of the ligature) [50].

2.7 Cell transfection

AC16 cells were seeded into culture plates and transfected when reaching 60–70% confluence. siRNA, miR-26a-5p mimics, inhibitor, negative control (NC), Lipofectamine® 3000 reagent, and Opti-MEM medium were combined in microcentrifuge tubes according to the manufacturer's recommended ratios, gently mixed, and incubated at room temperature for 5 min. The mixtures were then combined, gently mixed again, and incubated for an additional 15 min at room temperature. Cell culture medium was aspirated, and cells were washed twice with PBS before being replenished with basal medium. The transfection complexes were added to the culture dishes, followed by incubation at 37°C in a 5% CO_2 humidified incubator for 4–6 h. Subsequently, the basal medium was replaced with complete growth medium. The sequences of siRNAs are in Supplementary1.

2.8 RNA extraction and qRT-PCR analysis

Total RNA was extracted from cultured cells and engineered exosomes using an RNA extraction kit. First-strand cDNA was synthesized with a universal cDNA synthesis kit (Accurate Biotechnology, Hunan, China) according to the manufacturer's instructions. Expression of target genes was detected by quantitative real-time PCR using SYBR Green Master Mix on a fast real-time PCR system (PCR X960 Console). The relative expression of target genes was analyzed using the 2 − ΔΔCt method with U6 and β-actin as the internal reference. All primers used in this study were in Supplementary2.

2.9 Detection of ferroptosis-related indicators

Cell culture medium was aspirated, and cells were gently washed twice with ice-cold PBS. Serum-free medium containing 10 μM DCFH-DA was added, and cells were incubated at 37°C for 30 min in the dark. The probe solution was then removed, and cells were washed three times with PBS to eliminate non-internalized probe. The culture dishes were observed under an inverted fluorescence microscope (Thermo EVOS M5000, USA) to detect intracellular ROS levels.Serum and cellular samples were collected and processed according to the instructions of the corresponding assay kits. Reaction reagents were added sequentially, and absorbance was measured using a microplate reader. The levels of reduced glutathione (GSH), malondialdehyde (MDA), and superoxide dismutase (SOD) were calculated based on the formulas provided in the respective kit protocols[23, 24]. Ferrostatin-1 (Fer-1, 2 μM) was used as a positive control for ferroptosis inhibition in all relevant experiments.

2.10 Western Blot

Total protein was extracted from mouse myocardial tissues and AC16 cells using RIPA lysis buffer (Beyotime Institute of Biotechnology). Equal amounts of protein were separated by 10% SDS-PAGE and transferred onto PVDF membranes (Millipore). After blocking with 5% skim milk, the membranes were incubated overnight at 4°C with primary antibodies against CD9, CD81, TSG101, Alix, Flot1, Calnexin, MSMO1, GPX4, and β-actin (all diluted 1:2000). The following day, membranes were incubated with corresponding horseradish peroxidase-conjugated secondary antibodies for 1 h at room temperature. After washing with TBST, protein bands were visualized using an enhanced chemiluminescence (ECL) reagent. Band intensities were quantified using Image-J software, with β-actin serving as the loading control. The primary antibodies were used in this study were in Supplementary3.

2.11 Cardiac Function Assessment

ELISA kits were allowed to equilibrate to room temperature. Subsequently, 100 μL of standards or serum samples were added to each well, followed by the addition of 100 μL of horseradish peroxidase-conjugated detection antibody. The plate was sealed and incubated at 37°C for 60 min. After incubation, the reaction plate was washed five times with washing buffer and patted dry. Substrate solution was then added, and the plate was incubated again at 37°C for 15 min in the dark. The reaction was terminated by adding 50 μL of stop solution and mixing gently. Absorbance was measured using a microplate reader, and the levels of cardiac troponin I (cTnI) and creatine kinase-MB (CK-MB) in mouse

serum were calculated to evaluate the extent of myocardial injury. Serum samples from mice were processed according to the instructions provided with the GSH assay kit. Reaction reagents were added stepwise, and absorbance was recorded with a microplate reader. The concentration of reduced GSH in serum was calculated using the formula supplied with the kit to assess the antioxidative capacity.

2.12 Masson trichrome staining

Myocardial tissue sections from each group of mice were deparaffinized and immersed in potassium dichromate solution for 12 h. After washing with running water, sections were stained with Weigert's iron hematoxylin for 5 min, rinsed with distilled water, and then immersed in Masson's ponceau-acid fuchsin solution for 5 min. Sections were subsequently treated with 2 g/dL acetic acid for 3 min, followed by 1 g/dL phosphomolybdic acid for 3 min. Aniline blue solution (2 g/dL) was applied for 5 min, after which sections were immersed in 0.2 g/dL acetic acid for 3 min. Finally, sections were dehydrated through a graded ethanol series, cleared in xylene, mounted, and observed under a light microscope for image acquisition.

2.13 Bioinformatics analysis

Genomic sequencing data for myocardial ischemia-reperfusion, specifically from sample series GSE74951, were retrieved from the GEO database. Differential expression of miRNAs was analyzed and screened using Weishengxin analysis to investigate the role of differentially expressed miRNAs in myocardial ischemia-reperfusion injury. Bioinformatics approaches were further employed to predict upstream regulators of MSMO1 and to explore the relationship between MSMO1 and miR-26a-5p. The underlying principle is that a lower free energy of binding between the miRNA sequence and the mRNA sequence facilitates their interaction, thereby enabling miRNA-mediated regulation of the target gene. The gene sequences of miR-26a-5p and MSMO1 mRNA were obtained from the NCBI database. Target gene prediction was performed using TargetScan to examine the binding potential between MSMO1 and miR-26a-5p.

2.14 Statistical analysis

Experimental data were statistically analyzed using R software, and graphs were constructed with GraphPad Prism 10. Data are presented as mean ± standard deviation (SD). Multiple groups of samples were compared using one-way ANOVA if they followed normal distribution and homogeneity of variance. Differences between groups were assessed using the Student's *t*-test. A P-value < 0.05 was considered statistically significant.

3. Results

3.1Cholesterol Metabolism Regulates Iron Death in MIRI:

To systematically identify key regulators of ferroptosis in MIRI, we retrieved ferroptosis-related genes from the GeneCards database, KEGG PATHWAY Database, Gene Expression Omnibus database, and relevant publications. After preprocessing, a non-redundant set of 965 ferroptosis-associated genes was

obtained. Target genes were further acquired from the TargetScan, miRWalk, starBase, and miRDB databases, while ischemia-reperfusion (IR)-related genes were extracted from the GSE66360 dataset. Finally, 15 ferroptosis-linked proteins were identified in MIRI. Among them, the cholesterol-related protein MSMO1 caught our attention (Fig. 1A). To define the functional role of MSMO1, To define the functional role of MSMO1, we established a H/R model in AC16 cardiomyocytes. Strikingly, we discovered and validated for the first time the central role of MSMO1—a key enzyme in the cholesterol synthesis pathway—in regulating cardiomyocyte ferroptosis during MIRI. In the H/R model, cardiomyocytes exhibited typical ferroptotic features: compared with the control group and the ferroptosis inhibitor Fer-1 group which served as a positive control for ferroptosis suppression , the H/R group showed significantly elevated levels of MDA and ROS (Fig. 1B-C), while GSH content and SOD activity were markedly reduced (Fig. 1D-E). These results confirm that Fer-1 effectively blocks H/R-induced ferroptosis, establishing it as a valid tool for ferroptosis rescue experiments. Notably, we observed for the first time that during this process, both MSMO1 protein expression decreased synchronously and significantly (Fig. 1F-G), suggesting that the MSMO1 may be a key regulatory node of ferroptosis in MIRI.

To demonstrate the role of MSMO1 in counteracting ferroptosis during MIRI, we further constructed an MSMO1-knockdown (KO) cell model. Results showed that under H/R stress, MSMO1 knockdown exacerbated the ferroptotic process: compared with the H/R-only group, the MSMO1-KO group displayed more severe lipid peroxidation, higher ROS and MDA levels (Fig. 1H-I), and lower GSH and SOD levels (Fig.1J-K). This directly demonstrates that MSMO1 deficiency aggravates cardiomyocyte ferroptosis. Collectively, our findings align with and extend a recent report in Nature which identified the distal cholesterol synthesis pathway as an endogenous ferroptosis-suppressive system[14,15]. Notably, while the distal cholesterol biosynthesis pathway was recently identified as an endogenous ferroptosis-suppressive system, our study provides the first demonstration that this mechanism operates in the pathophysiological context of MIRI. We further pinpoint MSMO1 as a core regulator of ferroptosis in this specific setting and, for the first time, uncover its upstream miRNA regulator miR-26a-5p. Therefore, this study provides a novel theoretical framework and highlights MSMO1 as a potential therapeutic target for preventing or treating MIRI through the modulation of cholesterol metabolism.

3.2 miR 26a 5p is an upstream regulator of MSMO1

Building on our identification of MSMO1 as a key regulator in MIRI-associated ferroptosis, we next sought to elucidate its upstream regulatory mechanisms, focusing on non-coding RNAs. To this end, we employed an integrated approach combining bioinformatics analysis and targeted metabolomics. This investigation was conducted across cardiac tissues from MIRI mouse and rat models, as well as myocardial tissues and blood samples from clinical myocardial infarction patients. Data from the GEO database were analyzed, and differentially expressed genes in MIRI were filtered using a statistical threshold of $P < 0.05$. Among the candidates, miR-26a-5p was identified as being significantly

downregulated (Fig. 2A). This finding was subsequently validated at the cellular level: in the AC16 cell-based H/R model, qPCR results confirmed a marked decrease in miR-26a-5p expression compared to the control group (Fig. 2B). Furthermore, bioinformatic predictions using databases such as TargetScan revealed an evolutionarily conserved binding site for miR-26a-5p within the 3'UTR of MSMO1 mRNA (Fig. 2C), strongly suggesting that MSMO1 is a direct downstream target of miR-26a-5p. Collectively, these results imply that the downregulation of miR-26a-5p is closely associated with the pathological progression of MIRI. Although prior studies have indicated a protective role for miR-26a-5p in the cardiovascular system[25], its potential involvement in MIRI through the regulation of ferroptosis remained unexplored.

To directly test this bioinformatic prediction and elucidate the functional relationship, we performed gain- and loss-of-function experiments in cardiomyocytes. As illustrated in Fig. 2D-F, knockdown of miR-26a-5p led to a significant reduction in both MSMO1 protein levels and the content of its functional metabolite, 7-DHC. Conversely, overexpression of miR-26a-5p effectively reversed the H/R-induced downregulation of both MSMO1 and 7-DHC. These data conclusively demonstrate that miR-26a-5p positively regulates the expression of the MSMO1/7-DHC axis.

3.3 Engineered Exosomes Enable Efficient Loading and Delivery of miR-26a-5p

Prior to functional investigations, we systematically characterized the Exo isolated from MSCs to confirm their identity and establish a reliable foundation for subsequent experiments[26]. First, the morphology of the isolated vesicles was assessed by TEM. The images revealed that the vesicles displayed the characteristic cup-shaped or "disc-like" morphology typical of exosomes[27], with intact membrane structures and well-defined boundaries (Fig. 3A). Subsequently, NTA was performed for quantitative size distribution. The results showed that the particle diameters were predominantly distributed between 100-150 nm[28], with a peak around 100-120 nm, which falls within the expected size range for exosomes (Fig. 3B). To further confirm their molecular identity, we analyzed protein markers by western blotting. Notably, classical exosomal markers—including CD9, CD81, TSG101, Alix, and Flot1—were positively detected in the MSC-derived samples[29], whereas the endoplasmic reticulum marker Calnexin was absent (Fig. 3C). Together, these data validated the successful isolation of high-purity exosomes from MSCs, excluding significant contamination by cellular debris or other organelles. Building on this successful characterization, we next generated engineered exosomes. miR-26a-5p mimics were loaded into exosomes using an exosome-specific transfection reagent (Fig. 3D). Following total RNA extraction from equal volumes (150 μL) of native and engineered exosome preparations, qPCR analysis confirmed a significant increase in miR-26a-5p levels in the engineered exosomes compared with native exosomes (Fig. 3E). This relative quantification, normalized to exosomal U6 RNA, demonstrates a markedly higher miRNA loading efficiency in engineered exosomes. The result indicates successful miRNA loading and efficient cargo incorporation.

To evaluate the functional delivery capability of these engineered exosomes, we then examined their uptake by target cells. Exosomes were labeled with the fluorescent dye DiR and co-cultured with AC16 cells[30]. As shown by confocal microscopy, distinct red fluorescence signals were observed inside AC16 cells after incubation, with fluorescence overlapping the cytoplasmic region, demonstrating efficient internalization of the engineered exosomes (Fig. 3F). Subsequent qPCR analysis of total RNA extracted from AC16 cells revealed a significant elevation of intracellular miR-26a-5p levels in the engineered-exosome treatment group compared with both the native-exosome group and the blank control group (Fig. 3G). These results collectively confirm that the engineered exosomes serve as an efficient delivery vehicle, effectively transporting exogenous miR-26a-5p into recipient cardiomyocytes and enhancing its intracellular expression.

3.4 Engineered Exosomes Delivering miR-26a-5p Suppress Ferroptosis by Regulating the MSMO1/7-DHC Axis

Building on the demonstrated efficiency of engineered exosomes in delivering miR-26a-5p to cardiomyocytes, we next sought to determine whether this delivery system could confer functional protection against H/R-induced injury. To this end, we evaluated the effects of engineered exosomes on cellular oxidative stress and ferroptosis-related pathways in AC16 cells subjected to H/R[31]. Our results showed a significant protective effect. Compared with the H/R model group and the natural exosome treatment group, engineered exosome treatment significantly reduced cellular ROS accumulation (Fig. 4A) and decreased MDA levels, which is a key marker of lipid peroxidation (Fig. 4B). At the same time, relevant indicators of cellular antioxidant capacity were significantly restored: GSH content was markedly increased (Fig. 4C), and SOD activity was significantly enhanced (Fig. 4D). Notably, the degree of protection provided by engineered exosomes was superior to that of the Fer-1 treatment group and the natural exosome treatment group (Fig. 4A-D). Taken together, these findings suggest that miR-26a-5p delivered by engineered exosomes can effectively alleviate oxidative damage in cardiomyocytes under H/R stress.

To elucidate the underlying molecular mechanism, we further investigated key proteins in the cholesterol synthesis and ferroptosis regulatory axis. Western blot analysis showed that engineered-exosome treatment significantly upregulated the expression of both MSMO1 and GPX4, the latter being a central inhibitor of ferroptosis (Fig. 4E-F). Consistently, enzyme-linked immunosorbent assay confirmed a substantial increase in the intracellular content of the downstream metabolite 7-DHC following treatment (Fig. 4G).

In summary, these data support a mechanistic model wherein miR-26a-5p, delivered via engineered exosomes, targets MSMO1 to activate a cellular cholesterol synthesis branch. This promotes the production of 7-DHC, which in turn reinforces the GPX4-mediated antioxidant defense system. Ultimately, this cascade suppresses lethal lipid peroxidation and ferroptosis, thereby attenuating cardiomyocyte

injury induced by H/R. Our findings thus highlight the potential therapeutic value of exosome-based miR-26a-5p delivery for myocardial ischemia-reperfusion injury.

3.5 Engineered Exosomes Exhibit Cardiac Targeting In Vivo

To assess the in vivo targeting capability and therapeutic potential of engineered exosomes delivering miR-26a-5p for MIRI, we conducted a series of experiments in a mouse model. A murine MIRI model was established in C57BL/6 mice (Fig. 5A), with post-operative electrocardiography confirming the characteristic marked ST-segment elevation indicative of ischemic injury[32](Fig. 5B), and surgical images clearly demonstrated the whitening of the infarct area following coronary artery ligation (Fig. 5C-D), confirming the successful induction of ischemic injury. To visually track exosome distribution, unmodified exosomes Exo or engineered exosomes (Exo-miR-26a-5p) labeled with the near-infrared dye DiR were administered via tail-vein injection to I/R mice, alongside a PBS control. Real-time in vivo fluorescence imaging at 2 h and 4 h post-injection revealed a distinct targeting profile. Engineered exosomes showed rapid enrichment toward the ischemic region. By 4 h, fluorescence signal intensity in the thoracic (particularly cardiac) area was significantly stronger in the engineered-exosome group than in the unmodified-exosome group. In contrast, the latter displayed relatively higher background accumulation in mononuclear phagocytic organs such as the liver and spleen (Fig. 5E-F). For definitive confirmation, mice were euthanized at 24 h for ex vivo organ imaging. Strikingly, ex vivo heart images visually demonstrated the strongest overall fluorescence signal in the engineered-exosome group, with signal distribution closely corresponding to the ischemic area at risk (Fig. 5G). To quantitatively assess in vivo targeting efficiency, we measured the average fluorescence intensity (radiance) within standardized ROIs of the heart, liver, and spleen. The cardiac signal was significantly higher in the engineered-exosome group compared to the unmodified-exosome group ($p < 0.01$), while liver and spleen signals showed no significant difference between the two exosome groups. Semi-quantitative analysis of regional fluorescence intensity further confirmed that cardiac signals in the engineered-exosome group were significantly higher than in both the unmodified-exosome and PBS control groups (Fig. 5G). These data provide quantitative evidence that the engineering strategy enhances the targeting efficiency of exosomes to the ischemic myocardium.

3.6 Engineered Exosomes Delivering miR-26a-5p Effectively Ameliorate MIRI In Vivo

To systematically evaluate the therapeutic efficacy of engineered exosomes in vivo, we first assessed key markers of myocardial injury and systemic oxidative status. Compared with the sham group, mice subjected to I/R exhibited significantly elevated serum levels of cTnI and CK-MB, confirming substantial myocardial damage[35]. Administration of unmodified Exo via tail-vein injection resulted in a statistically significant reduction in both markers. Notably, treatment with Exo-miR-26a-5p further and more potently lowered the concentrations of cTnI and CK-MB, demonstrating a superior therapeutic effect compared to

unmodified exosomes (Fig. 6A-B).Given the central role of ferroptosis and oxidative stress in I/R injury, we next evaluated the systemic antioxidant capacity[36]. As expected, serum GSH levels dropped sharply following I/R[37]. Importantly, exosome treatment-particularly with engineered exosomes-effectively reversed this decline, significantly restoring serum GSH content (Fig. 6C). This graded protective effect suggested that miR-26a-5p delivered by engineered exosomes synergistically enhances the inherent cardioprotective properties of exosomes and bolsters systemic antioxidant defenses. We then evaluated long-term tissue repair and remodeling. Masson's trichrome staining of heart sections revealed that I/R injury induced marked interstitial collagen deposition[38]. While unmodified exosome intervention partially reduced the fibrotic area, engineered-exosome treatment exhibited a more pronounced suppressive effect on fibrosis and better preserved myocardial tissue architecture (Fig. 6D). Quantitative analysis confirmed that the percentage of fibrotic area in the engineered-exosome group was significantly lower than in all other I/R-treated groups.

To elucidate the underlying molecular mechanism responsible for this protection, we examined the expression of key proteins in the myocardial tissue. RT-qPCR analysis showed that I/R injury strongly suppressed the expression of both MSMO1 and GPX4. Unmodified exosomes moderately upregulated GPX4 but had a limited effect on MSMO1. In contrast, engineered-exosome treatment simultaneously and markedly increased the myocardial expression levels of both MSMO1 and GPX4 (Fig. 6E), a finding highly consistent with our in vitro results. Finally, to directly confirm successful target engagement, qPCR analysis of myocardial miR-26a-5p expression confirmed that mice treated with engineered exosomes had significantly higher cardiac levels of miR-26a-5p than all other groups (Fig. 6F). This result conclusively demonstrates that the engineered exosomes successfully deliver functional miR-26a-5p to the target tissue in vivo and effectively elevate its expression.

4. Discussion

This study not only systematically reveals a novel regulatory axis in myocardial ischemia-reperfusion injury-the miR-26a-5p/MSMO1/7-DHC axis-but, more importantly, successfully develops and validates a targeted therapeutic strategy based on engineered mesenchymal stem cell-derived exosomes, thereby achieving a transition from mechanistic exploration to potential therapeutic application. First, the central protective role of the distal cholesterol biosynthesis pathway in MIRI was established. In both cellular and animal models, the levels of MSMO1 and its metabolite 7-DHC were positively correlated with cardiomyocyte survival and cardiac function. This finding aligns closely with the groundbreaking concept recently reported in Nature that "the distal cholesterol synthesis pathway constitutes an endogenous ferroptosis-suppression system,"and it explicitly positions this fundamental biological mechanism within the critical clinical pathology of MIRI[14, 15].

We further demonstrated that loss of MSMO1 function exacerbates ferroptosis, whereas supplementation with its upstream activator alleviates injury, thereby validating this axis as an effective intervention target. The core breakthrough of this research lies in elucidating the upstream regulatory mechanism of this pathway. We found that miR-26a-5p is significantly downregulated in MIRI. The

deficiency of miR-26a-5p in MIRI represents a key upstream event leading to impaired MSMO1/7-DHC axis function and increased susceptibility to ferroptosis. In addition, Interestingly, we observed that in the MIRI model, both miR-26a-5p and MSMO1 were down-regulated synchronously at the mRNA and protein levels; however, in functional rescue experiments, transfection of miR-26a-5p mimic led to an up-regulation of MSMO1 expression. Although the dual-luciferase reporter assay confirmed that miR-26a-5p can bind to the 3'-UTR of MSMO1 and suppress its reporter activity—indicating a direct targeting relationship—this inhibitory effect was not reflected as a decrease in MSMO1 protein in intact cells, but rather as an increase. This paradoxical observation indicates that the net regulatory output of miR-26a-5p on MSMO1 is not simply a direct repression; instead, we propose an indirect regulatory mechanism involving an unknown intermediate factor X, i.e., miR-26a-5p → X → MSMO1, where X is a negative regulator of MSMO1 that is suppressed by miR-26a-5p. Consequently, the indirect up-regulatory effect outweighs the direct inhibition. This model explains why miR-26a-5p overexpression increases MSMO1 expression despite the direct binding site. Importantly, this indirect regulation does not negate the functional relevance of the miR-26a-5p/MSMO1 axis; our data demonstrate that MSMO1 is a key downstream effector, as evidenced by the correlation between MSMO1 levels and ferroptosis susceptibility. Future studies using MSMO1-specific rescue or knockout experiments (e.g., overexpression of MSMO1 lacking the 3'UTR) would further establish the necessity and sufficiency of MSMO1 in mediating the protective effects of miR-26a-5p. [39–41].

Linking non-coding RNA regulatory networks to metabolic anti-cell-death defense mechanisms offers a new perspective for understanding the complex regulation of MIRI[42]. However, translating this mechanistic insight into a therapeutic strategy faces common challenges associated with therapeutic nucleic acids-such as miRNA mimics-including low delivery efficiency, poor stability, and lack of target specificity in vivo[43–44]. To address these limitations, we adopted engineered exosomes as a delivery platform. Our data indicate that engineered exosomes loaded with miR-26a-5p possess multiple advantages: 1) Efficient loading and protection: miR-26a-5p mimics were successfully encapsulated into the exosomal lumen, effectively shielding them from degradation by serum nucleases. 2) Enhanced targeting: In vivo imaging revealed that engineered exosomes exhibited significantly greater enrichment in the ischemic myocardium compared with native exosomes, likely attributable to the homing properties of exosomal membrane proteins in the specific pathological microenvironment. 3) Synergistic therapeutic effect: Beyond delivering miR-26a-5p, the engineered exosomes may also carry other beneficial paracrine factors that act in concert with the loaded miRNA. Consequently, they outperform native exosomes in restoring cardiac function (as reflected by reduced cTnI/CK-MB levels), suppressing adverse remodeling (attenuated fibrosis), and enhancing systemic antioxidant capacity (elevated GSH levels)[45–46].

It is important to address the apparent discrepancy between the protective role of 7-DHC reported here and its well-documented toxicity in Smith-Lemli-Opitz syndrome (SLOS), where 7-DHC accumulation leads to developmental defects[52, 53]. This duality can be explained by several factors. First, in SLOS, 7-DHC accumulates chronically from embryonic stages, reaching high concentrations that disrupt

membrane integrity and signaling. In contrast, in acute MIRI, the increase in 7-DHC is transient and localized, likely acting as a rapid adaptive response to oxidative stress. Second, the pathophysiological context differs markedly: SLOS involves multiple organ systems with impaired cholesterol synthesis, whereas in MIRI, the overall cholesterol pool remains largely intact, and 7-DHC specifically exerts its anti-ferroptotic effect by acting as a radical-trapping antioxidant[14, 55]. Third, 7-DHC is the most oxidizable lipid molecule reported to date, with a propagation rate constant for free radical peroxidation that is 200 times that of cholesterol[54, 56]; it can protect against ferroptosis at low to moderate levels through radical-trapping activity, but its excessive accumulation leads to the formation of cytotoxic oxysterols that contribute to SLOS pathology[55, 56]. Thus, our findings do not contradict the SLOS literature but rather highlight the context-dependent nature of 7-DHC function.

The findings of this study carry significant translational implications. First, they propose a potential novel combined therapeutic strategy: targeting ferroptosis by simultaneously enhancing the classic GPX4 pathway (e.g., using Fer-1) and the MSMO1/7-DHC metabolic pathway uncovered here may yield additive or synergistic cardioprotective effects. Second, our engineered exosome platform provides a proof-of-concept for precise intervention at the time of reperfusion. In the future, it may be feasible to explore catheter-based delivery of engineered exosomes directly into the coronary arteries during PCI, enabling therapeutic intervention with spatiotemporal precision[33].

This study has several limitations that should be acknowledged. First, although the mouse model provides robust mechanistic evidence, cardiac physiology and coronary architecture differ between mice and humans. Validation in a large-animal MIRI model (e.g., porcine) represents a critical step toward preclinical translation[34]. Second, the cardiac targeting efficiency of exosomes remains suboptimal and could be further improved. Future studies may explore surface functionalization with ischemia-specific homing peptides (e.g., peptides targeting ICAM-1 or VCAM-1) or encapsulation within “smart” materials responsive to the ischemic myocardial microenvironment, to enhance targeting specificity and therapeutic efficacy[47]. Third, the observation period in this study is relatively short. The long-term safety, immunogenicity, and impact on the development of chronic heart failure following engineered-exosome treatment warrant more comprehensive evaluation. Fourth, although our engineered exosomes were administered immediately at the onset of reperfusion, the clinically relevant scenario for MI patients often requires treatment given after reperfusion. We acknowledge that we have not systematically evaluated the therapeutic window for post-reperfusion administration. Future studies should define the optimal time window for translation. Fifth, while our bioinformatic and functional data support MSMO1 as a key target of miR-26a-5p, miRNAs typically regulate dozens of genes. We cannot completely exclude the possibility that other miR-26a-5p targets contribute to the observed protective effects. Future genome-wide target profiling or rescue experiments with MSMO1 mutants lacking the 3'UTR would help establish specificity.

5. Conclusion

In summary, we have delineated a novel signaling pathway in MIRI through which miR-26a-5p suppresses ferroptosis by regulating the MSMO1/7-DHC metabolic axis. More importantly, we successfully developed a safe and efficient engineered-exosome delivery system capable of precisely restoring this axis both in vitro and in vivo, thereby effectively mitigating myocardial injury. This work not only deepens the understanding of the pathological mechanisms underlying MIRI, but also lays a solid experimental foundation for the development of next-generation cardiovascular therapies based on non-coding RNcAs and extracellular vesicles.

Declarations

Author Contribution Statement

Yonglin Fu: Conceptualization, writing original draft, and experimental index detection. Bingjie Han: Data analysis and statistics. Lu Liu: Animal model construction. Wenjie Chen: Partial western blot. Ciying Kuang: Bioinformatics data analysis. Mei Jiang: Format and content review. Xiaojun Cui: Review and project funding.

Funding Declaration

This work was supported by the General Program of the Natural Science Foundation of Xinjiang Uygur Autonomous Region (No.2023D01A61), the Characteristic Innovation Project of Ordinary Universities in Guangdong Province (No.2020KTSCX046).

Acknowledgments

This work was supported by the General Program of the Natural Science Foundation of Xinjiang Uygur Autonomous Region (No.2023D01A61), the Characteristic Innovation Project of Ordinary Universities in Guangdong Province (No.2020KTSCX046)

Conflicts of Interest

The authors declare that the research was conducted in the absence of any commercial or financial relationships that could be construed as a potential conflict of interest.

References

1. Chen J, Xu C, Qiu L, et al. Heparin administration at first medical contact vs immediately before primary percutaneous coronary intervention: the HELP-PCI trial. *Eur Heart J*. 2025;46(39):3888-3901.
2. Yu C, Chen Y, Luo H, et al. NAT10 promotes vascular remodelling via mRNA ac4C acetylation. *Eur Heart J*. 2025;46(3):288-304.

3. Qu Z, Pang X, Mei Z, et al. The positive feedback loop of the NAT10/Mybbp1a/p53 axis promotes cardiomyocyte ferroptosis to exacerbate cardiac I/R injury. Redox Biol. 2024;72:103145.
4. Tsurusaki S, Kizana E. Mechanisms and Therapeutic Potential of Multiple Forms of Cell Death in Myocardial Ischemia-Reperfusion Injury. *Int J Mol Sci*. 2024;25(24):13492.
5. Stockwell BR. Ferroptosis turns 10: Emerging mechanisms, physiological functions, and therapeutic applications. *Cell*. 2022;185(14):2401-2421.
6. Saini HK, Arneja AS, Dhalla NS. Role of cholesterol in cardiovascular dysfunction. *Can J Cardiol*. 2004;20(3):333-346.
7. Luo J, Yang H, Song BL. Mechanisms and regulation of cholesterol homeostasis. *Nat Rev Mol Cell Biol*. 2020;21(4):225-245.
8. Da Dalt L, Cabodevilla AG, Goldberg IJ, Norata GD. Cardiac lipid metabolism, mitochondrial function, and heart failure. *Cardiovasc Res*. 2023;119(10):1905-1914.
9. Girod WG, Jones SP, Sieber N, Aw TY, Lefer DJ. Effects of hypercholesterolemia on myocardial ischemia-reperfusion injury in LDL receptor-deficient mice. *Arterioscler Thromb Vasc Biol*. 1999;19(11):2776-2781.
10. Zhang J, Wu S, Xu Y, et al. Lipid overload meets S-palmitoylation: a metabolic signalling nexus driving cardiovascular and heart disease. *Cell Commun Signal*. 2025;23(1):392.
11. Liepinsh E, Zvejniece L, Clemensson L, et al. Hydroxymethylglutaryl-CoA reductase activity is essential for mitochondrial β-oxidation of fatty acids to prevent lethal accumulation of long-chain acylcarnitines in the mouse liver. *Br J Pharmacol*. 2024;181(16):2750-2773.
12. Dominiak K, Galganski L, Budzinska A, Jarmuszkiewicz W. Coenzyme Q deficiency in endothelial mitochondria caused by hypoxia; remodeling of the respiratory chain and sensitivity to anoxia/reoxygenation. *Free Radic Biol Med*. 2024;214:158-170.
13. Budzinska A, Jarmuszkiewicz W. The Cellular and Mitochondrial Consequences of Mevalonate Pathway Inhibition by Nitrogen-Containing Bisphosphonates: A Narrative Review. *Pharmaceuticals (Basel)*. 2025;18(7):1029.
14. Li Y, Ran Q, Duan Q, et al. 7-Dehydrocholesterol dictates ferroptosis sensitivity. *Nature*. 2024;626(7998):411-418.
15. Freitas FP, Alborzinia H, Dos Santos AF, et al. 7-Dehydrocholesterol is an endogenous suppressor of ferroptosis. Nature. 2024;626(7998):401-410.
16. Li J, Sun S, Zhu D, et al. Inhalable Stem Cell Exosomes Promote Heart Repair After Myocardial Infarction. Circulation. 2024;150(9):710-723.
17. Whiteside TL. Biology of extracellular vesicles and the potential of tumor-derived vesicles for subverting immunotherapy of cancer. J Immunother Cancer. 2025;13(1):e010376.
18. Mirgh D, Sonar S, Ghosh S, et al. Landscape of exosomes to modified exosomes: a state of the art in cancer therapy. *RSC Adv*. 2024;14(42):30807-30829.

19. Wang X, Chen W, Zeng W, et al. Extracellular vesicles as biomarkers and drug delivery systems for tumor. *Acta Pharm Sin B*. 2025;15(7):3460-3486.
20. Kostyusheva A, Romano E, Yan N, Lopus M, Zamyatnin AA Jr, Parodi A. Breaking barriers in targeted Therapy: Advancing exosome Isolation, Engineering, and imaging. Adv Drug Deliv Rev. 2025;218:115522.
21. Yang X, Cao X, Xu X, et al. Diagnostic value of circulating miRNA-26a-5p, miRNA-21-5p, and miRNA-191-5p in elderly patients with acute myocardial infarction. Chin J Evid Based Cardiovasc Med. 2024;16(3):288-291,295.
22. Wang Y, Guo R, Lu Y, et al.Experimental study on the effects of Hu Huang extract on hypoxia/reoxygenation-induced cardiomyocyte apoptosis and oxidative stress via the miR-26a-5p/NF-κB pathway. J Chin Med Mater. 2024;47(1):208-213.
23. Yin M, Li S, Liu M, et al. GUCY1A1-LDHA Axis Suppresses Ferroptosis in Cardiac Ischemia-Reperfusion Injury. Circ Res. 2025;137(7):986-1005.
24. Leng L, Li P, Liu R, et al. The main active components of Prunella vulgaris L. alleviate myocardial ischemia-reperfusion injury by inhibiting oxidative stress and ferroptosis via the NRF2/GPX4 pathway. J Ethnopharmacol. 2025;345:119630.
25. Cui F. Expression of miR-26a-5p in plasma of patients with acute heart failure and its relationship with short-term prognosis. Labeled Immunoassays Clin Med. 2022;29(4):608-612,651.
26. Leng L, Li P, Liu R, et al. The main active components of Prunella vulgaris L. alleviate myocardial ischemia-reperfusion injury by inhibiting oxidative stress and ferroptosis via the NRF2/GPX4 pathway. J Ethnopharmacol. 2025;345:119630.
27. Chen P, Ruan A, Zhou J, et al. Extraction and identification of synovial tissue-derived exosomes by different separation techniques. J Orthop Surg Res. 2020;15(1):97. Published 2020 Mar 9.
28. Chen C, Zhang Z, Gu X, Sheng X, Xiao L, Wang X. Exosomes: New regulators of reproductive development. Mater Today Bio. 2023;19:100608.
29. Ferroni L, D'Amora U, Gardin C, et al. Stem cell-derived small extracellular vesicles embedded into methacrylated hyaluronic acid wound dressings accelerate wound repair in a pressure model of diabetic ulcer. J Nanobiotechnology. 2023;21(1):469.
30. Lázaro-Ibáñez E, Faruqu FN, Saleh AF, et al. Selection of Fluorescent, Bioluminescent, and Radioactive Tracers to Accurately Reflect Extracellular Vesicle Biodistribution in Vivo. ACS Nano. 2021;15(2):3212-3227.
31. Zhang Z, Yang J, Zhou Q, et al. The role and mechanism of the cGAS-STING pathway-mediated ROS in apoptosis and ferroptosis induced by manganese exposure. Redox Biol. 2025;85:103761.
32. Welt FGP, Batchelor W, Spears JR, et al. Reperfusion Injury in Patients With Acute Myocardial Infarction: JACC Scientific Statement. J Am Coll Cardiol.
33. Ren Y, Wang W, Yu C, et al. An injectable exosome-loaded hyaluronic acid-polylysine hydrogel for cardiac repair via modulating oxidative stress and the inflammatory microenvironment. Int J Biol Macromol. 2024;275(Pt 2):133622.

34. Boengler K, Buechert A, Heinen Y, et al. Cardioprotection by ischemic postconditioning is lost in aged and STAT3-deficient mice. Circ Res. 2008;102(1):131-135.
35. Zhu M, Zhao T, Zha B, et al. Piceatannol protects against myocardial ischemia/reperfusion injury by inhibiting ferroptosis via Nrf-2 signaling-mediated iron metabolism. Biochem Biophys Res Commun. 2024;700:149598.
36. Tan M, Yin Y, Chen W, et al. Trimetazidine attenuates Ischemia/Reperfusion-Induced myocardial ferroptosis by modulating the Sirt3/Nrf2-GSH system and reducing Oxidative/Nitrative stress. Biochem Pharmacol. 2024;229:116479.
37. Wang F, Wang X, Wang C, et al. Gut microbiota-derived glutathione from metformin treatment alleviates intestinal ferroptosis induced by ischemia/reperfusion. BMC Med. 2025;23(1):285.
38. Wang YC, Zhu Y, Meng WT, et al. Dihydrotanshinone I improves cardiac function by promoting lymphangiogenesis after myocardial ischemia-reperfusion injury. Eur J Pharmacol. 2025;989:177245.
39. Hausser J, Zavolan M. Identification and consequences of miRNA-target interactions--beyond repression of gene expression. Nat Rev Genet. 2014;15(9):599-612.
40. Kelly TJ, Brümmer A, Hooshdaran N, Tariveranmoshabad M, Zamudio JR. Temporal Control of the TGF-β Signaling Network by Mouse ESC MicroRNA Targets of Different Affinities. Cell Rep. 2019;29(9):2702-2717.e7.
41. Zhuang C, Wang P, Huang D, et al. A double-negative feedback loop between EZH2 and miR-26a regulates tumor cell growth in hepatocellular carcinoma. Int J Oncol. 2016;48(3):1195-1204.
42. Kim D. LOXL1-AS1/miR-761/PTEN as a Novel Signaling Pathway in Myocardial Ischemia and Reperfusion Injury (MIRI): Epigenetic Regulation by Long Non-Coding RNA (LncRNA) in MIRI. Korean Circ J. 2023;53(6):404-405.
43. Jin Y, Han G, Gao Y, et al. Serum-tolerant polymeric complex for stem-cell transfection and neural differentiation. Nat Commun. 2025;16(1):2022.
44. Yueh PF, Chiang IT, Weng YS, et al. Innovative dual-gene delivery platform using miR-124 and PD-1 via umbilical cord mesenchymal stem cells and exosome for glioblastoma therapy. J Exp Clin Cancer Res. 2025;44(1):107.
45. Wang C, Zhao C, Wang W, Liu X, Deng H. Biomimetic noncationic lipid nanoparticles for mRNA delivery. Proc Natl Acad Sci U S A. 2023;120(51):e2311276120.
46. Jiang Y, Li S, Shi R, et al. A Novel Bioswitchable miRNA Mimic Delivery System: Therapeutic Strategies Upgraded from Tetrahedral Framework Nucleic Acid System for Fibrotic Disease Treatment and Pyroptosis Pathway Inhibition. Adv Sci (Weinh). 2024;11(1):e2305622.
47. Guo W, Chen H, Liu F, Chen B, Liu C, Cai Y. Peptide amphiphiles alleviate myocardial endoplasmic reticulum stress to enhance cardiomyocyte-macrophage communication and promote macrophage M2 polarization. J Control Release. 2025;378:719-734.
48. Venturella M, Navaei A, Zocco D. Comprehensive Characterization and In Vitro Functionality Study of Small Extracellular Vesicles Isolated by Different Purification Methods from Mesenchymal Stem Cell

Cultures. *Int J Mol Sci*. 2025;26(21):10602.

49. Jiang X, Wang Y, Zhang X, et al. Melatonin-engineered MSCs-exosomes deliver USP4 to stabilise ARNTL and inhibit clock rhythmic ferroptosis for enhanced flap survival. *Clin Transl Med*. 2026;16(1):e70565.
50. Yang J, Yun X, Zheng W, et al. Nanoscale engineered exosomes for dual delivery of Sirtuin3 and insulin to ignite mitochondrial recovery in myocardial ischemia-reperfusion. *J Nanobiotechnology*. 2025;23(1):439.
51. Lange T, Maron L, Weber C, Biedenweg D, Schlüter R, Endlich N. Efficient delivery of small RNAs to podocytes in vitro by direct exosome transfection. *J Nanobiotechnology*. 2025;23(1):373.
52. Yu H, Patel SB. Recent insights into the Smith-Lemli-Opitz syndrome. Clin Genet. 2005;68(5):383-391.
53. Boland MR, Tatonetti NP. Investigation of 7-dehydrocholesterol reductase pathway to elucidate off-target prenatal effects of pharmaceuticals: a systematic review. Pharmacogenomics J. 2016;16(5):411-429.
54. Xu L, Porter NA. Free radical oxidation of cholesterol and its precursors: Implications in cholesterol biosynthesis disorders. Free Radic Res. 2015;49(7):835-849.
55. Cui S, Ye J. 7-Dehydrocholesterol: A sterol shield against an iron sword. Mol Cell. 2024;84(7):1183-1185.
56. Xu L, Porter NA. Reactivities and products of free radical oxidation of cholestadienols. J Am Chem Soc. 2014;136(14):5443-5450.

Figures

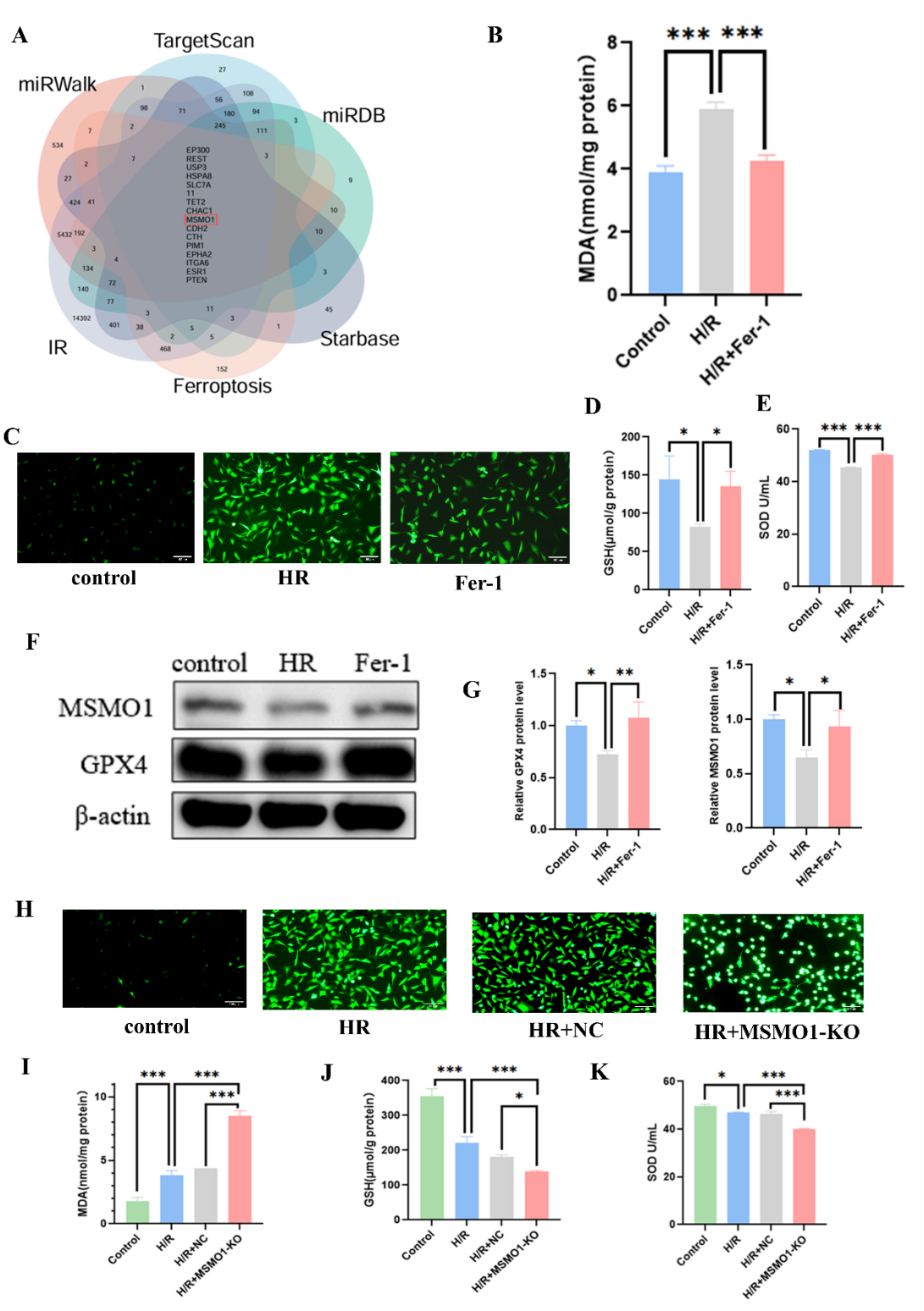


Figure 1

Identification of MSMO1 as a key regulator of ferroptosis in MIRI.

(A) Screening workflow for ferroptosis-associated genes in MIRI. MSMO1, a cholesterol synthesis pathway enzyme, was identified as a protein of interest. **(B-E)**Cardiomyocytes subjected to H/R exhibit typical ferroptosis hallmarks: increased levels of MDA (B) and ROS (C), and decreased GSH content (D)

and SOD activity (E) compared with control and Ferrostatin-1 treated groups. **(F-G)**Protein expression of MSMO1 is synchronously and significantly downregulated in H/R-injured cardiomyocytes. **(H-K)** Knockdown of MSMO1 exacerbates H/R-induced ferroptosis, further elevating MDA (H) and ROS (I) levels while reducing GSH (J) and SOD (K) levels compared with H/R alone.Data are presented as mean ± SD (n=3); *$p < 0.05$, **$p < 0.01$, ***$p < 0.001$.

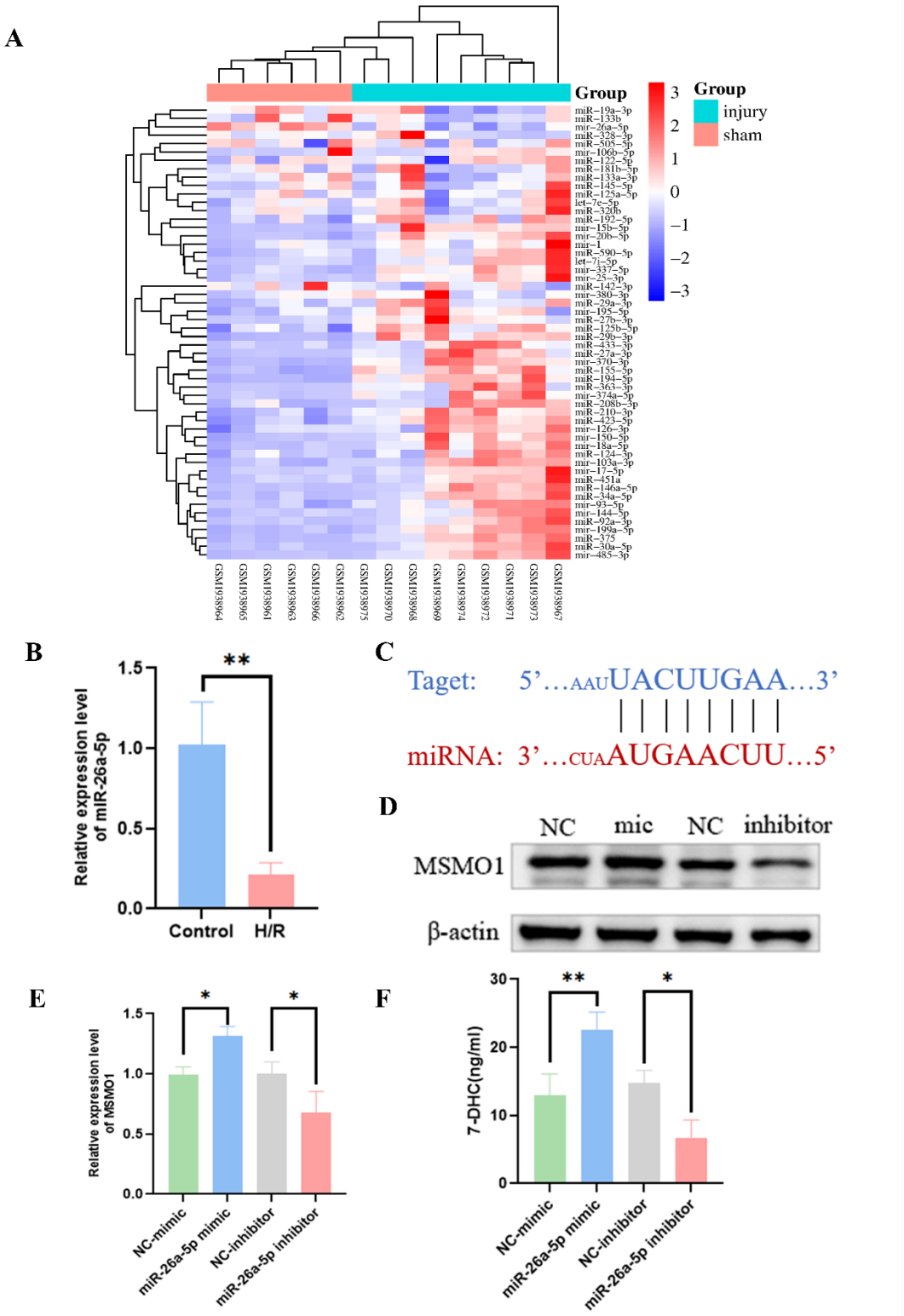


Figure 2

miR-26a-5p is downregulated in MIRI and targets MSMO1.

(A) Differential expression analysis of miRNAs in cardiac tissues from MIRI mice and rats, and clinical myocardial infarction samples. miR-26a-5p was significantly downregulated. **(B)** qPCR validation of miR-26a-5p expression in AC16 cells subjected to H/R. **(C)** Predicted conserved binding site between miR-26a-5p and the 3' UTR of MSMO1 mRNA. **(D-F)** Effects of miR-26a-5p knockdown and overexpression on MSMO1 protein expression and 7-DHC content in cardiomyocytes under H/R conditions.Data are represented as mean ± SD (n=3); *p< 0.05, **p < 0.01, ***p < 0.001.

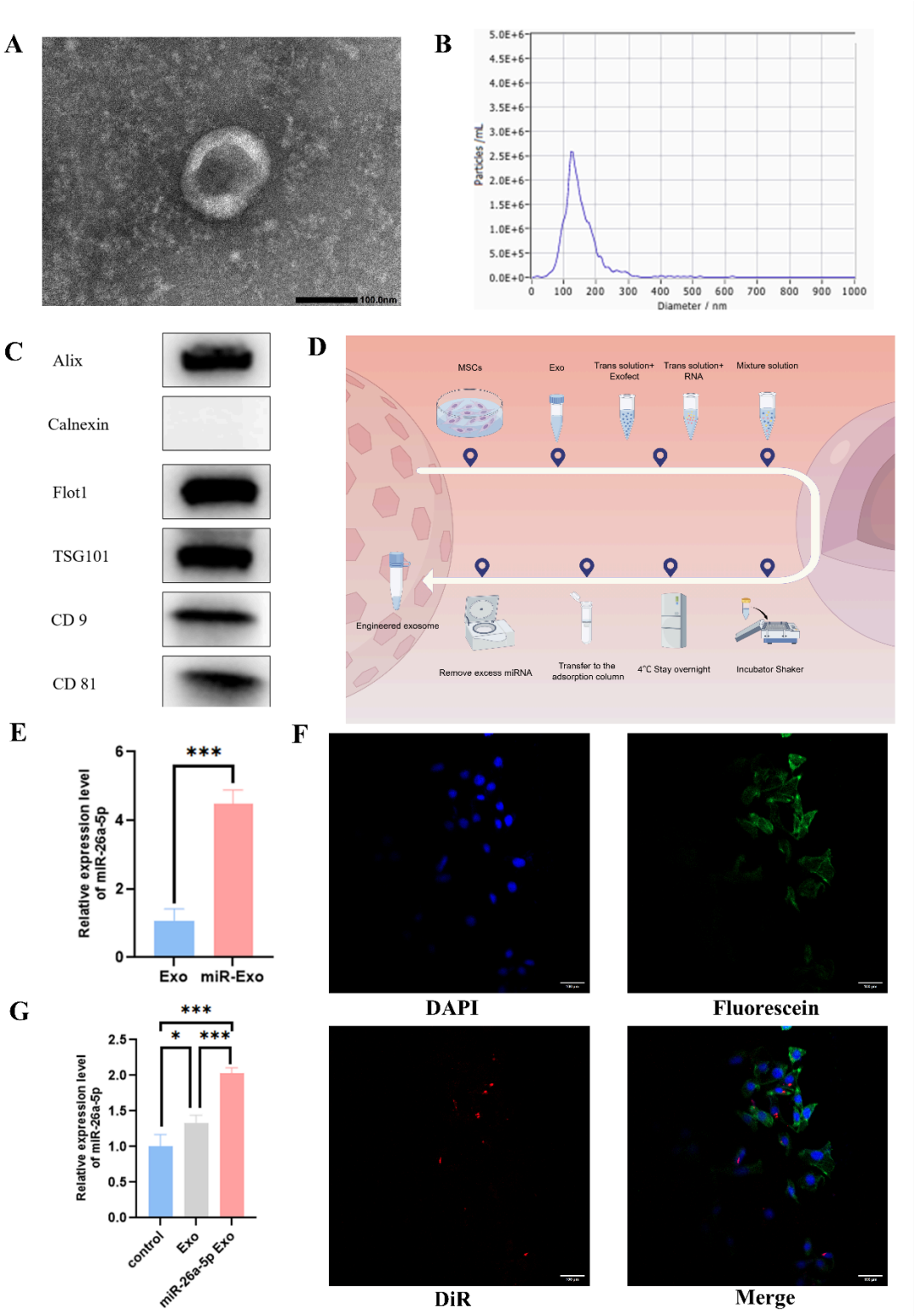


Figure 3

Characterization and Engineering of Exosomes.

(A) TEM image showing the typical cup-shaped morphology of isolated MSC-derived exosomes. **(B)** NTA analysis indicating that the diameter of extracted vesicles predominantly falls within the 100–150 nm range. **(C)**Western blot analysis confirming the presence of exosomal markers (CD9, CD81, TSG101, Alix, Flot1) and the absence of the endoplasmic reticulum marker Calnexin. **(D)** Schematic illustration of the

preparation of engineered exosomes loaded with miR-26a-5p mimics. **(E)** qPCR analysis demonstrating significantly elevated levels of miR-26a-5p in engineered exosomes compared to native exosomes. **(F)** Confocal microscopy images showing DiR-labeled engineered exosomes (red) internalized by AC16 cells. **(G)** qPCR analysis confirming increased intracellular levels of miR-26a-5p in AC16 cells treated with engineered exosomes. Data are represented as mean ± SD (n=3); *p< 0.05, **p < 0.01, ***p < 0.001.

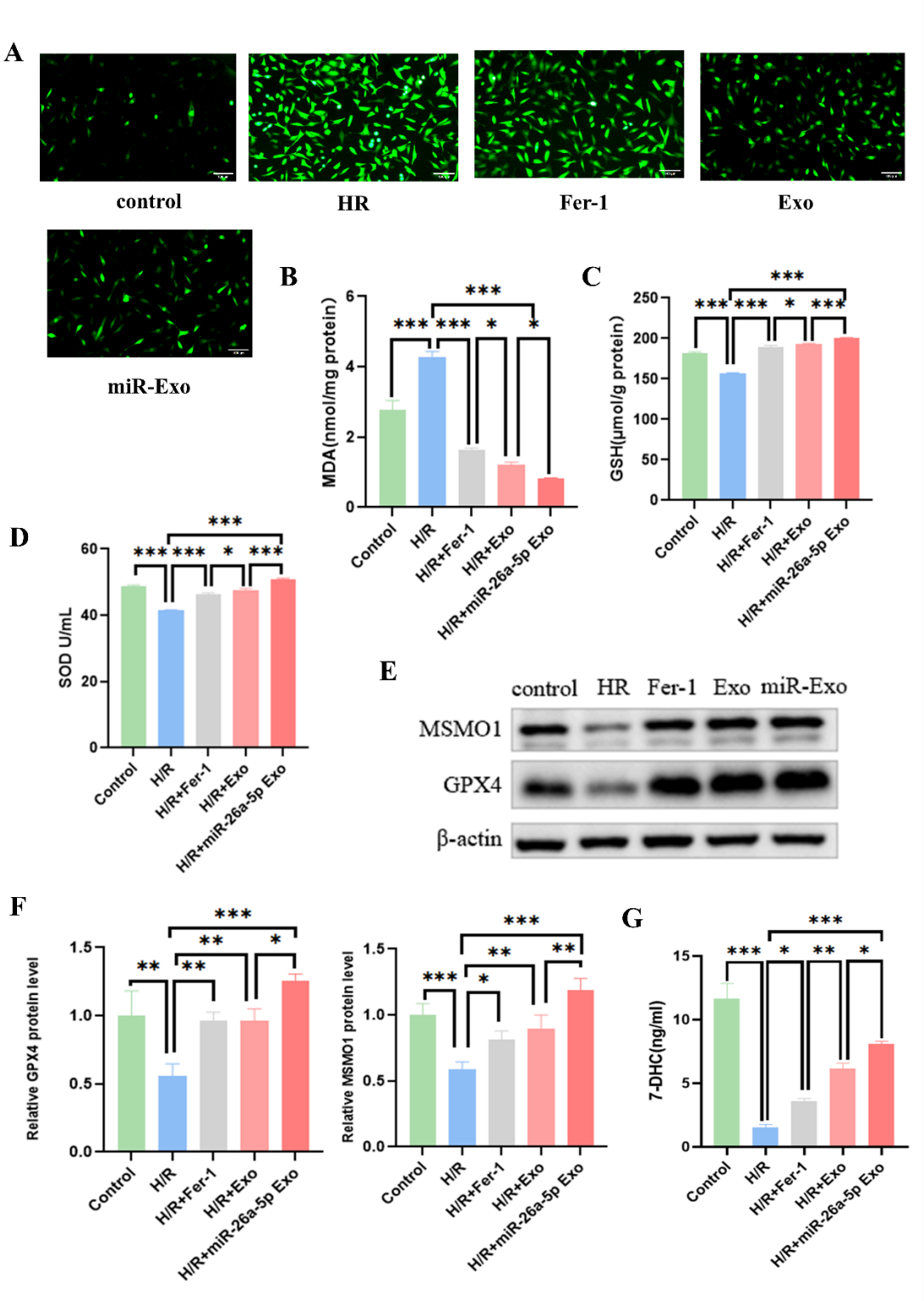


Figure 4

miR-26a-5p-enriched exosomes alleviate cardiomyocyte ferroptosis via MSMO1.

(A) Intracellular ROS accumulation was significantly reduced in AC16 cells treated with engineered exosomes compared to the H/R and native-exosome groups. **(B)**Lipid peroxidation marker MDA was markedly suppressed by engineered-exosome treatment. **(C-D)** Antioxidant capacity was restored, as shown by increased GSH content (C) and enhanced SOD activity (D). **(E-F)** Western blot analysis revealed upregulation of MSMO1 and GPX4 protein levels in the engineered-exosome group. **(G)** ELISA confirmed a significant increase in the intracellular content of the cholesterol synthesis metabolite 7-DHC. Data are represented as mean ± SD (n=3); *p< 0.05, **p < 0.01, ***p < 0.001.

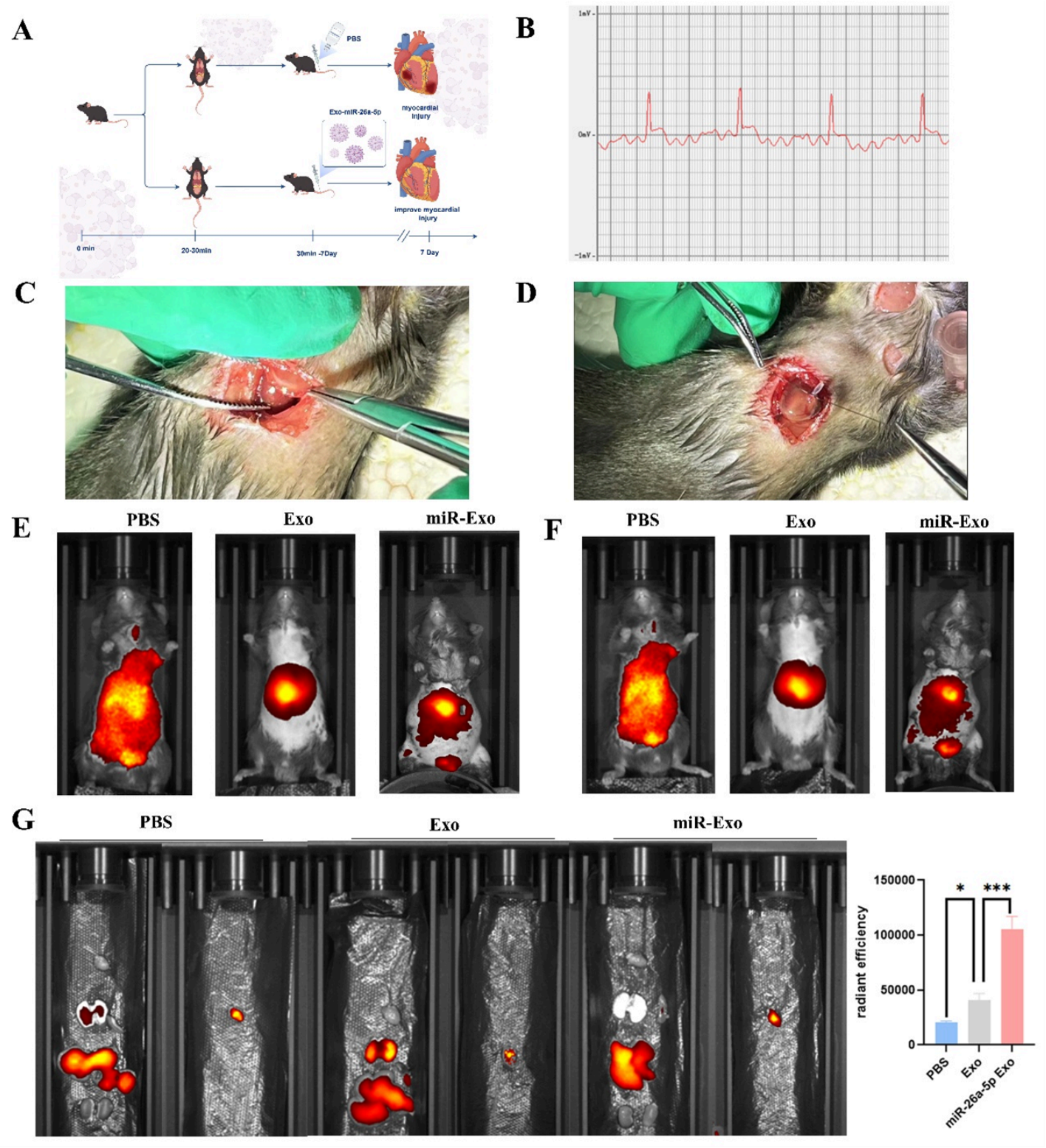


Figure 5

Cardiac-targeted delivery of engineered exosomes in MIRI.

(A) Schematic illustration of the murine MIRI model. **(B)** Representative electrocardiogram showing marked ST-segment elevation post-surgery. **(C-D)** Preoperative and postoperative mouse myocardial infarction surgery images. **(E-F)** In vivo fluorescence imaging at 2 h and 4 h post-injection of DiR-labeled

exosomes. Exo-miR-26a-5p show enhanced accumulation in the thoracic region compared to unmodified Exo. **(G)** In vivo fluorescence imaging of harvested organs (heart, liver, spleen, lungs, kidneys) at 24 h post-injection. Ex vivo heart images and semi-quantitative analysis of fluorescence intensity confirm significantly higher cardiac signals in the engineered-exosome group. Data are represented as mean ± SD (n=3); *p< 0.05, **p < 0.01, ***p < 0.001.

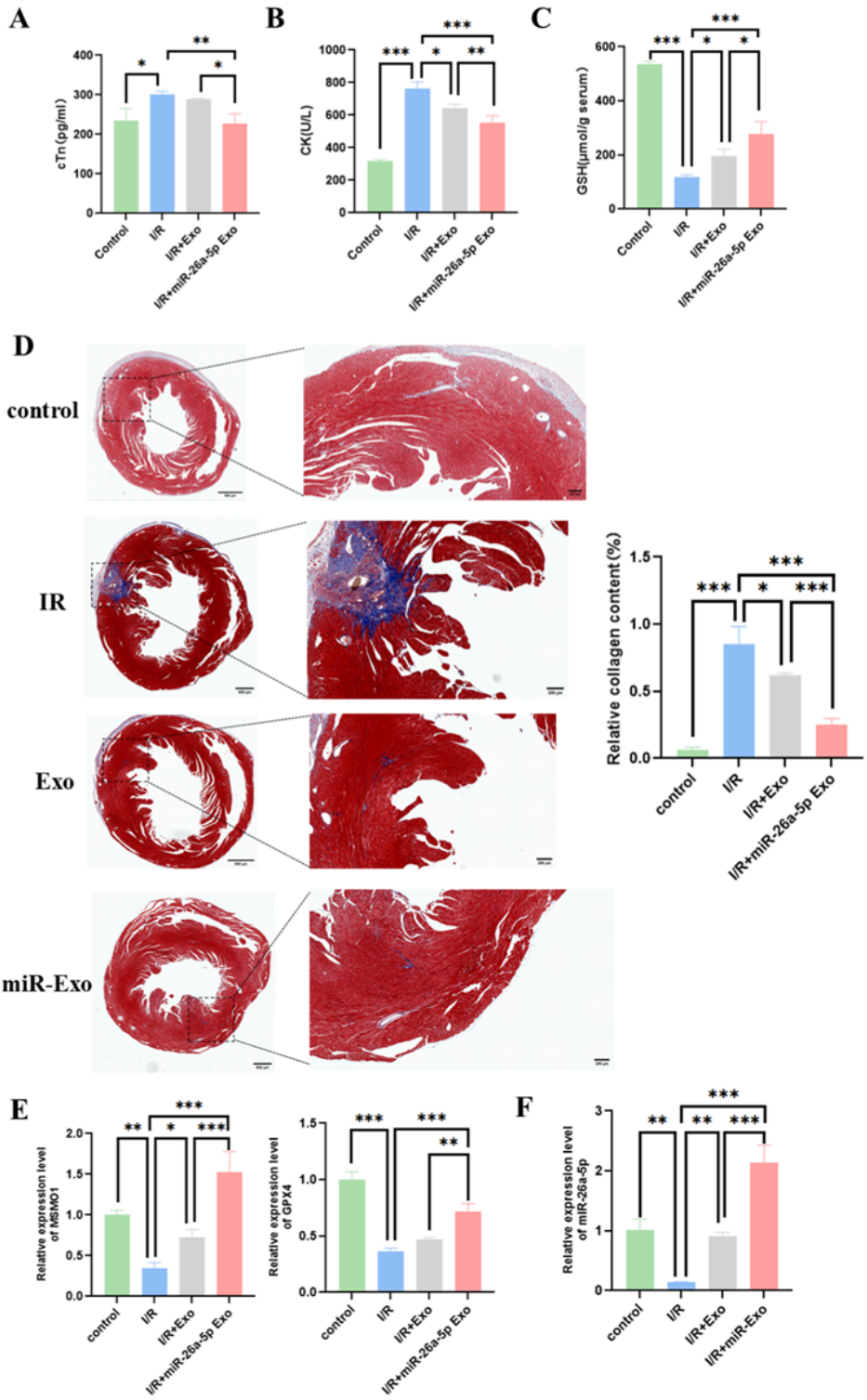


Figure 6

Therapeutic exosomes can mitigate cardiac injury.

(A-B) Serum levels of cardiac injury markers cTnI (A) and CK-MB (B) were significantly elevated after I/R; treatment with unmodified Exo reduced both markers, and Exo-miR-26a-5p further lowered their concentrations. **(C)** Serum GSH content was restored by exosome treatment, with the engineered-exosome group showing the most pronounced increase. **(D)** Representative Masson's trichrome staining of heart sections and quantitative analysis of fibrotic area; engineered-exosome treatment most effectively attenuated collagen deposition. **(E)** RT-qPCR analysis of myocardial tissue showing that Exo-miR-26a-5p simultaneously upregulated mRNA expression of MSMO1 and GPX4. **(F)** qPCR confirmation of elevated cardiac miR-26a-5p levels in the engineered-exosome group. Data are represented as mean ± SD (n=3); *p< 0.05, **p < 0.01, ***p< 0.001.

Supplementary Files

This is a list of supplementary files associated with this preprint. Click to download.

- Supplement1.docx
- Supplement2.docx
- Supplement3.docx
- GraphicalAbstract.docx